Journal of Structural Geology, Vol. 13, No. 8, pp. 945 to 953, 1991
Printed in Great Britain

0191-8141/91 $03.00+0.00

SEM electron channelling analysis of dynamic recrystallization in a quartz grain

GEOFFREY E. LLOYD

Department of Earth Sciences, University of Leeds, Leeds LS2 9JT, U.K.

and

BRETT FREEMAN

Badley, Ashton and Associates, Winceby House, Winceby, Lincolnshire LN9 6PB, U.K.

(*Received* 5 *October* 1990; *accepted in revised form* 22 *February* 1991)

Abstract—The SEM electron channelling (EC) technique has been used to investigate the processes involved in the dynamic recrystallization of an individual quartz porphyroclast. By using a combination of crystal-axis pole-figure diagrams and theoretical crystal-axes dispersion paths for individual crystal slip systems, it is possible to establish whether a relationship exists between recrystallized grains and parental grain. It is then possible to distinguish between rotational and migrational dynamic recrystallization processes, and to establish a dynamic recrystallization history for the porphyroclast. Dynamic recrystallization initiates as a subgrain rotation process. Initial rotation is accommodated by slip on individual systems leading to grain bending, elongate polygonal subgrains and a systematic orientation relationship between subgrains and parent. Larger rotations and neoblast formation require more than one slip system, but a systematic relationship between grains and parent can still be recognized. Rotational recrystallization produces an unstable microstructure, which is stabilized by grain-boundary migration.

INTRODUCTION

DYNAMIC recrystallization occurs to minimize strain energy during deformation via two processes (Drury *et al.* 1985, Urai *et al.* 1986): *grain-boundary migration* and *subgrain* or *grain rotation*. Both processes typically result in similar microstructures. However, where migration originates from the surrounding grains, the crystallographic orientation of any new grains will be controlled by the neighbouring grains and their texture represents a sample from the bulk rock texture. In contrast, rotated new grains are derived from the parent grain and their texture depends principally on this grain, although neighbouring grains with variable mechanical properties must have some influence due to the heterogeneity of deformation on the grain scale. Thus, a distinction between these two different processes requires a complete crystallographic description of the relationships between parent grain, subgrains and new grains. Such a description can now be made via the scanning electron microscope (SEM) electron channelling (EC) technique.

The SEM/EC technique (Joy *et al.* 1982, Lloyd 1987, Lloyd *et al.* in press) is capable of providing two types of image: (1) *orientation contrast* of crystal microstructure; and (2) *electron channelling patterns* (ECP) which accurately define the crystal orientation of grains, subgrains, etc., relative to specimen geometry. Although the spatial resolution of electron channelling patterns (ECPs) is nominally ~10 μm, it can be improved (Hall & Skinner 1978) to ~1 μm. The interpretation of SEM/EC crystal-orientation determination has also been improved by the use of the *CHANNEL* computer program (Schmidt & Olesen 1989).

We have chosen for our study a relatively pure quartzite (Dalradian Crinan Grits, SW Highlands of Scotland). Field evidence (Freeman 1985) indicates syn-deformational greenschist facies (370–400°C) metamorphism. We have confined our attention to a sample cut parallel to the XZ section of the finite strain ellipsoid ($X \geq Y \geq Z$). Optical microscopy shows that quartz grain-sizes are bimodally distributed between finer matrix (diameters $\leq$50 μm) and coarser porphyroclasts (diameters $\leq$1000 μm). The latter contain abundant rutile inclusions which allow the determination of the absolute amount of recrystallization. Using the method described by Freeman (1984), we find 12% of the total rock volume consists of new grains (neoblasts), with a 37% reduction in the volume of porphyroclasts. We discuss here results for only one porphyroclast ('Grain B'), although we have examined a representative selection from the range of dynamically recrystallized microstructures present.

SEM ELECTRON CHANNELLING OBSERVATIONS

The grain chosen for investigation (Figs. 1a & b) shows ~50% recrystallization and contains two distinct textural regions: a mantle of neoblasts and a core of subgrains. We obtained ECPs from 52 neoblast and subgrain regions (individually labelled in Fig. 1c) and derived from them the principle crystal-axes pole figures (Fig. 2). Each of these figures displays small clusters

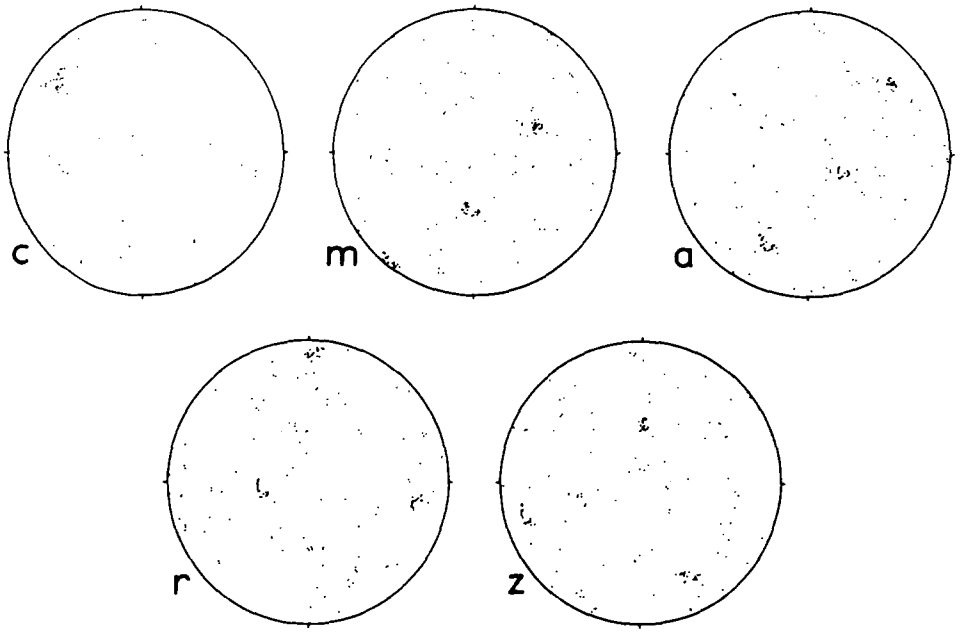

Fig. 2. ECP/*CHANNEL* derived pole figures (*c*, *m*, *a*, *r* and *z* crystal axes) of porphyroclast recrystallization texture. Tectonic axes: *X*, E–W; *Y*, vertical; *Z*, N–S.

against a background of scattered data points. The clusters are defined by the closely oriented core subgrains, whilst the scattered points are due to the more widely varying orientations of the mantle neoblasts.

Core subgrains

These define the 'single crystal' orientation of the host grain (Fig. 2; see also Table 1), with a tendency for dispersion in two directions (i.e. away from our representative host, **38**, towards **33** and **45**, respectively). The systematic change (Fig. 3) in both azimuth and plunge of the ECP/subgrain-normal directions indicates an overall curvature of (0001) basal planes across the grain core, such that the *c* axes occupy a narrow segment of a great circle dipping at about 10°. This progression in misorientation can be explained by bending and subgrain polygonization about the original orientation, accommodated by slip on a single crystal system. We therefore consider subgrain **38** to be representative of the original porphyroclast orientation. However, across the boundary between the core subgrains and mantle neoblasts, there is (usually) a major change in orientation. The more irregular orientations of subgrains close to this boundary (Fig. 3) probably involve a second slip system and herald the formation of mantle neoblasts (see below).

Mantle neoblasts

Neoblast grains generally have large misorientations relative to the original porphyroclast orientation (Fig. 2). Nevertheless, we have been able to recognize several distinct orientation relationships (see Table 1), as follows.

(1) *Group B*1. A single coincidence in either *m* (**B1a**) or *a* (**B1b**) with subgrain **38**, but >10° *c*-axis misorientation.

(2) *Group B*2. A coincidence in *c*, *m* and *a* with subgrain **38**.

(3) *Group B*3. Coincident *c* with subgrain **38**, and dispersion of *a* and *m* along the great circle defined by the basal plane of the porphyroclast.

(4) *Group B*4. Remaining neoblasts with no immediately obvious simple relationship to the porphyroclast.

These orientation relationships depict the dispersion paths away from the host porphyroclast orientation during recrystallization. In turn, this strongly suggests that dynamic recrystallization of this porphyroclast occurred via rotational rather than migrational processes. We must now identify the specific crystal slip systems responsible for these rotations.

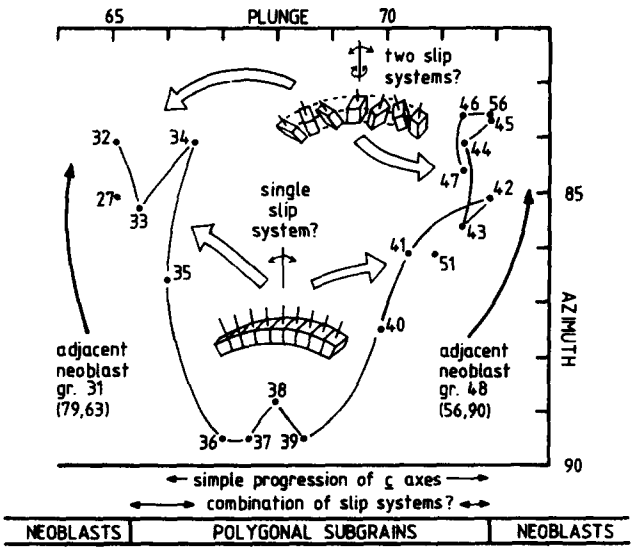

Fig. 3. Progressive misorientation of core subgrain orientations defined by azimuth and plunge of ECP (subgrain) normal directions.

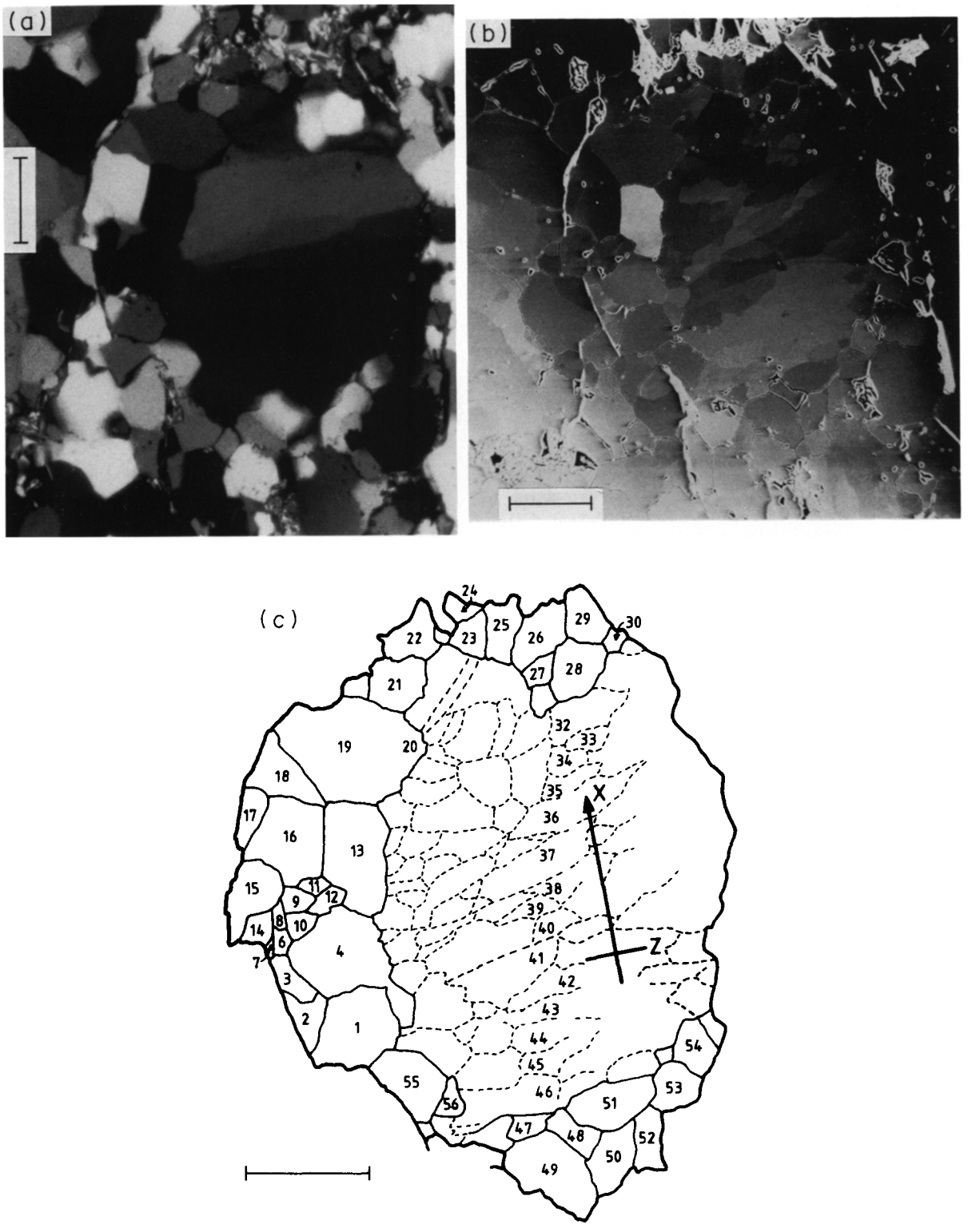

Fig. 1. The 50% dynamically recrystallized quartz porphyroclast ('Grain B') used in this study; note the subgrain core and neoblast mantle microstructures. All scale bars 200 μm. (a) Optical photomicrograph. (b) SEM/EC orientation contrast photomicrograph (30 kV accelerating voltage). (c) Location map showing positions of core subgrains (**32–47**) and mantle neoblasts (**1–31, 48–56**) from which ECPs were obtained.

Table 1. Coincidence relationships between parent porphyroclast (P), core subgrains (S) and mantle neoblasts (N) crystal axes: *, coincident; +, slight dispersion; b, dispersion in porphyroclast basal plane; exceptionally large neoblasts in **bold**. GRP refers to slip system identification

		Crystal axes									Crystal axes						
			m			*a*						*m*			*a*		
No.	GRP	*c*	1	2	3	1	2	3	No.	GRP	*c*	1	2	3	1	2	3
N01	B3	*	b	b	b	b	b	b	N31	B1b						+	
N02	B1a			*					S32		*	*	*	*	*	*	*
N03	B3	*	b	b	b	b	b	b	S33		*	*	*	*	*	*	*
N04	B3	+	b	b	b	b	b	b	S34		*	*	*	*	*	*	*
N07	B3	+	b	b	b	b	b	b	S35		*	*	*	*	*	*	*
N10	B3	+	b	b	b	b	b	b	S36		*	*	*	*	*	*	*
N11	B3	+	b	b	b	b	b	b	S37		*	*	*	*	*	*	*
N12	B3	+	b	b	b	b	b	b	S38		P	P	P	P	P	P	P
N13	B1a				+				S39		*	*	*	*	*	*	*
N14	B1b							*	S40		*	*	*	*	*	*	*
N15	B1b							*	S41		*	*	*	*	*	*	*
N16	B1a			+					S42		*	*	*	*	*	*	*
N17	B1b							*	S43		*	*	*	*	*	*	*
N18	B1a		*				+		S44		*	*	*	*	*	*	*
N19	B4								S45		*	*	*	*	*	*	*
N20	B4								S46		*	*	*	*	*	*	*
N21	B4								S47		*	*	*	*	*	*	*
N22	B1b	+	+	+	+	*	+	+	N48	B1a		+					
N23	B4								N49	B1b					+		
N24	B4								N50	B1a		*					
N25	B4								N51	B2	*	*	*	*	*	*	*
N26	B2	*	*	*	*	*	*	*	N52	B1a		+					
N27	B2	*	*	*	*	*	*	*	N53	B1a		*					
N28	B1b						*		N54	B1a		+					
N29	B1a					*			N55	B1a		*					
N30	B4								N56	B2	*	*	*	*	*	*	*

DETERMINATION OF CRYSTAL SLIP SYSTEMS

We can use the crystal-axis pole figures (Fig. 2) to determine active slip systems, as follows. For a progressive rotational misorientation each slip system maintains distinctive relationships between crystal axes, slip plane and slip direction. It is these relationships which are responsible for the dispersion patterns of the crystal axes. As we demonstrate, relationships between the crystal axes recognized by SEM/EC can usually be explained by slip on either basal-plane or 'basal-prism' systems (Fig. 4).

Slip on basal-plane systems constrains the pole to the slip plane (i.e. *c*) and the specific slip direction (e.g. *m* or *a*) to move along great circles. The pole to this great circle must therefore be a constant axis of rotation (e.g. *a* or *m*). The remaining *a* and *m* axes must move along small circles. In practice, there are three potential slip directions, and hence three potential rotation axes, for each of these basal plane slip systems (i.e. **M1–3, A1–3).**

The permutations offered by the three slip directions lead to more complex dispersion patterns. Thus, for simplicity, we shall consider only single rotation axes (Figs. 4a & b), using the single crystal orientation indicated by the core subgrains as the origin for the dispersions. For example, basal-*m* slip parallel to **M3** (Fig. 4a) is indicated by the following crystal-axes distributions: a single *a* cluster about the **A2** rotation axis; a

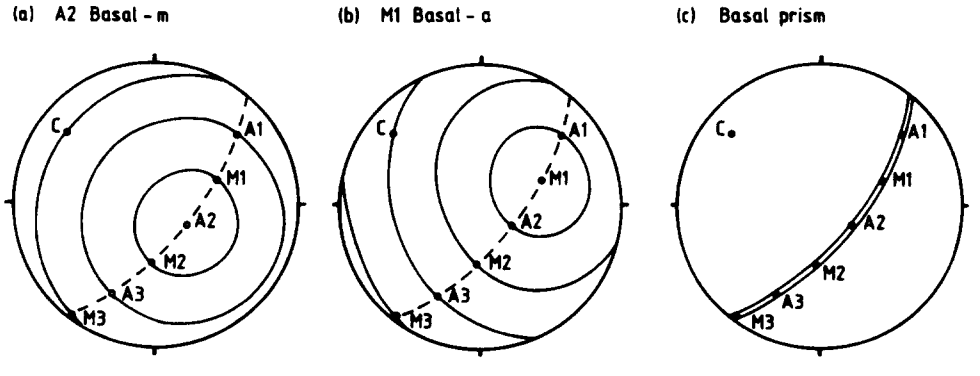

Fig. 4. Examples of crystal slip systems responsible for specific orientation relationships (dispersion patterns) between porphyroclast, subgrains and neoblasts crystal axes, assuming the same initial orientation of crystal axes as 'Grain B' (**C, M1–3** and **A1–3** indicate the positions of the *c*, *m* and *a* crystal axes). (a) Dispersion paths for **M3** basal-*m* slip centred on **A2**. (b) Dispersion paths for **A3** basal-*a* slip centred on **M1**. (c) Undifferentiated basal prism slip systems (e.g. prism-*a* and prism-*m*).

dispersion of *c* and *m* along the great circle through **C** and **M3**; and small circle dispersions of the other *a* and *m* through **A1–3** and **M1–2**, respectively. In contrast, basal-*a* slip parallel to **A3** (Fig. 4b) is indicated by: a single *m* cluster about the **M1** rotation axis; a dispersion of *c* and *a* along the great circle through **C** and **A3**; and small circle dispersions of the other *m* and *a* through **M2–3** and **A1–2**.

Slip on 'basal-prism' systems constrains the slip direction and the pole to the prism plane (which must lie in the basal plane) to a great-circle distribution. The *c* axis therefore must be a constant axis of rotation. Such slip systems always result in coincident *c* clusters and dispersions of *a* and *m* within a great circle defined by the original basal plane (Fig. 4c). Thus, crystal-axis pole figures are unable to distinguish between individual basal-prism slip systems (e.g. between prism-*a* and prism-*m*).

ACTIVE SLIP SYSTEMS

Comparison between the crystal-axes dispersion patterns summarized in Fig. 4 and our SEM/EC observations (Fig. 2 and Table 1) should help determine the crystal slip systems active in this porphyroclast. We assume that the original orientation of the porphyroclast is defined by the core subgrains. This in turn defines the positions of the potential rotation axes for each slip system (see Fig. 4): i.e. **C**, single *c* axis position; **M1–3**, three *m* axes positions; and **A1–3**, three *a* axes positions. However, to illustrate more clearly the dispersion paths for the generally small amounts of data involved, we have used the approach suggested by Lloyd *et al.* (in press) to derive contoured *c*, *m* and *a* axes pole figures from the *true* (i.e. even plus odd) orientation distribution functions (ODF) calculated from the discrete ECP data. This approach clearly shows the overall orientation distributions (Fig. 5a), the approximate single crystal orientation defined by the core subgrains (Fig. 5b), and the scatter representing the mantle neoblasts (Fig. 5c). We now consider separately the crystal slip systems responsible for these distributions.

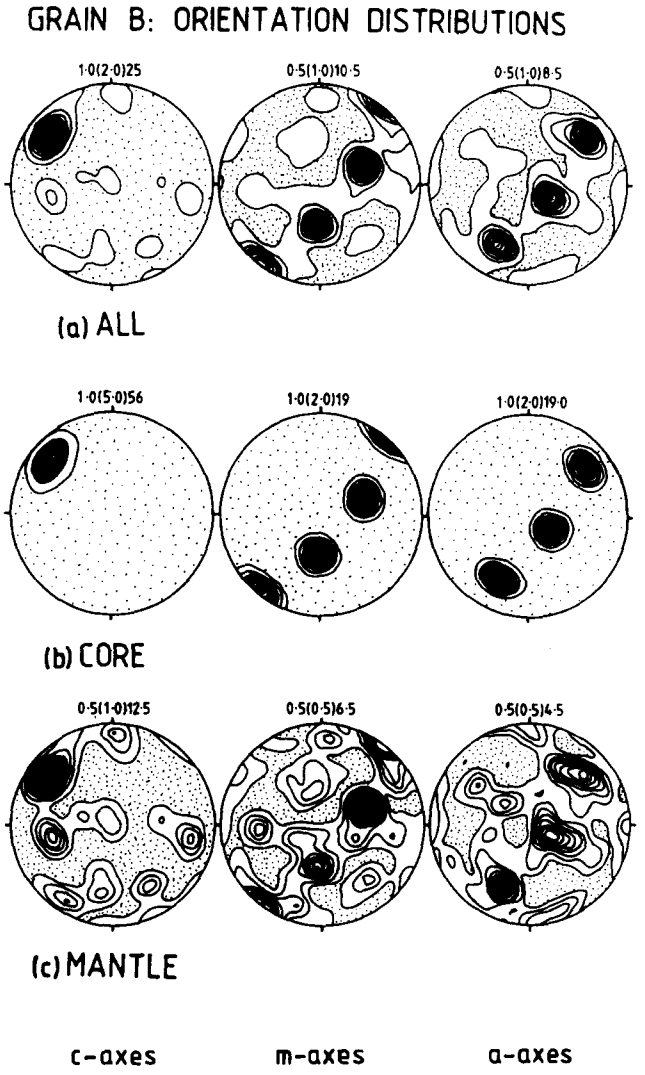

Fig. 5. Principle crystal axes (*c*, *m* and *a*) pole figures derived from the true ODF calculated from the discrete ECP data. The contours are defined by: minimum (interval) maximum values, stipple indicates frequencies less than the minimum contour. Tectonic axes: *X*, E–W; *Y*, vertical, *Z*, N–S. (a) All data (core subgrains and mantle neoblasts). (b) Core subgrains. This clustered distribution is consistent with polygonization involving **A3** basal-*a* slip centred on **M1**. (c) Mantle neoblasts, showing a dispersed distribution due to the operation of several crystal slip systems (see Figs. 6–8).

Core subgrains

The crystal-axes pole figures (Fig. 5b) show slight, bidirectional dispersions from the porphyroclast orientation, indicated by the shape of the contour clusters. The **M1** cluster shows the minimum dispersion, whilst the **C–A3** elliptical clusters are elongate within their common great circle. These observations are consistent with the subgrains having developed by **A3** basal-*a* slip centred on **M1**, which accommodated polygonization via bending about, and relative to, subgrain **38** (which therefore represents the orientation of the parental porphyroclast).

Mantle neoblasts

The crystal textures of neoblasts show much more complex dispersion patterns (Fig. 5c) than the core subgrains. However, we have already seen that several distinct groupings can be recognized (Table 1). Each of these groups indicates deformation on a different crystal slip system and/or a different recrystallization process. We therefore further divide the neoblast data into these different groups and derive contoured *c*, *m* and *a* axes pole figures (Fig. 6) from their true orientation distribution functions.

Group B1a is represented by (Fig. 6a): **M1** cluster; **M2–M3** and **A1–A2** small circles; and **C–A3** great circle. This dispersion pattern is consistent with **A3** basal-*a* slip

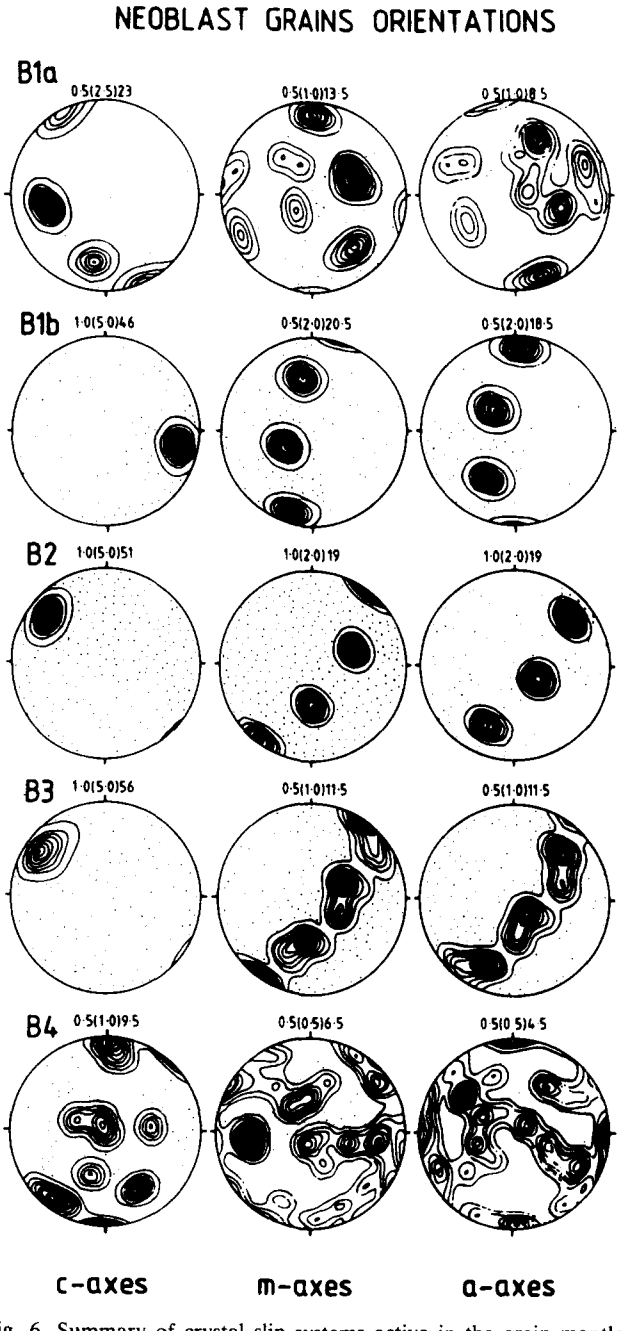

Fig. 6. Summary of crystal slip systems active in the grain mantle region during dynamic recrystallization. Tectonic axes: *X*, E–W; *Y*, vertical; *Z*, N–S. (a) *Group B1a* neoblasts: **A3** basal-*a* slip about **M1**. (b) Group *B1b* neoblasts: **M1** basal-*m* slip about **A3** (after initial subgrain polygonization via **A3** basal-*a* slip about **M1**). (c) *Group B2* neoblasts: polygonization involving **A3** basal-*a* slip about **M1**. (d) *Group B3* neoblasts: 'basal-prism' slip system(s). (e) *Group B4* neoblasts with complex distributions. Note the 'density maximum' in the *m*-axis pole figure (see Fig. 7).

centred on **M1**. *Group B1b* is represented by a somewhat ambiguous distribution (Fig. 6b), but the following relationships can be recognized: a cluster slightly displaced from **A3**; **A1–A2** and **M2–M3** small circles; and **C–M1** great circle. This dispersion pattern is consistent with **M1** basal-*m* slip centred on a displaced **A3**. The direction of dispersion suggests that slip preferentially exploited the 'subgrain **38** towards subgrain **45**' polygonization system. It is also significant that the displacement of the *a* cluster occurs on the great circle distribution produced by basal-*a* slip. This suggests that basal-*m* slip occurred after basal-*a* slip (including core subgrain polygonization).

Group B2 neoblasts show (Fig. 6c) only slight dispersion of all crystal axes, with an **M1** minimum dispersion and a partial **C–A3** great circle. The dispersions are in two directions away from the original orientations. This pattern is identical to that shown by the core subgrains (Fig. 5b) and suggests that these 'neoblasts' are actually subgrains which have been preserved within the mantle. They have developed by subgrain polygonization involving **A3** basal-*a* slip centred on **M1**.

Group B3 neoblasts exhibit (Fig. 6d) a **C** cluster and a combined **M1–3**, **A1–3** great circle. This dispersion pattern is consistent with 'basal-prism' slip centred on **C**, although we have been unable to determine the precise slip system(s).

Group B4 (Fig. 6e) neoblasts are significantly dispersed from the porphyroclast/subgrains orientations (Figs. 2, 5b and 6c). This suggests more complex recrystallization histories, although the weakly defined clusters of certain axes suggest common dispersion paths involving several slip systems for some neoblasts. For example, consider the *m*-axis cluster represented by the 'density maximum'. This consists of neoblasts **19–21**, but their complete 'single crystal'orientations comprise two configurations (Fig. 7a). These different orientations with coincident *m*-axes can be produced by the following dispersion sequence (Fig. 7b): 1. **A3** basal-*a* slip centred on **M1**; 2. **M3** basal-*m* slip centred on the modified **A2** position; and 3. **A1** basal-*a* slip centred on the now doubly modified **M2** position. The final step is responsible for the separation of the two neoblast orientations (except for the common **M2** *m*-axis) because it operates in opposite (i.e. axial) directions, perhaps in a similar manner to the initial bending about subgrain 38.

Most of the crystallographic data are inconsistent with grain-boundary migration as a major recrystallization mechanism. However, the textures of the exceptionally large and unpolygonized neoblasts (e.g. **4, 13, 16, 19** and **20**) suggest that some grain-boundary migration has occurred. These neoblasts share no common crystal axes (Fig. 8) and hence their orientations cannot be explained by a common rotational recrystallization history. Clearly, since these neoblasts represent the largest overall, they are large relative to neoblasts which share the same slip-system characteristics. A simple explanation is that these large neoblasts have undergone grain growth via grain-boundary migration. For **13, 16, 19** and **20**, this probably occurred at the expense of neighbouring neoblasts. However, **4** is almost surrounded by neoblasts with similar orientations and/or crystal slip system histories. It is possible that this region initially consisted of an array of subgrains which subsequently formed a single neoblast via migration of subgrain boundaries. The remnant of this subgrain array may be represented by neoblasts **3, 7, 10–12**.

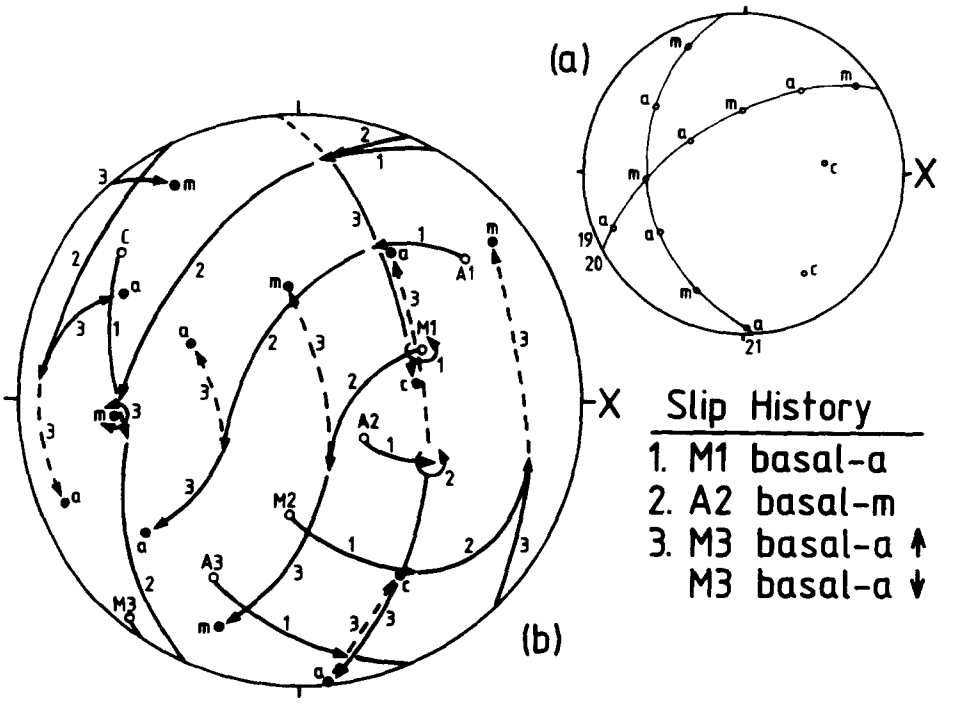

Fig. 7. Explanation of *Group* 4 neoblasts (tectonic axes: *X*, E–W; *Y*, vertical; *Z*, N–S). (a) Neoblasts **19**, **20** and **21** are dispersed from the parental orientations (see Fig. 5b) and from each other apart from a common *m* axis. (b) Slip system history of neoblasts **19–21**: 1. **A3** basal-*a* slip about **M1**; 2. **M3** basal-*m* slip about a modified **A2**; and 3. **A1** basal-*a* slip about a doubly-modified **M2**, in opposite (axial) directions.

CONCLUSIONS

Our SEM/EC analyses confirm the suggestions made by several earlier workers (e.g. Hobbs 1968, Ransom 1971, Wilson 1973) that the dynamic recrystallization of an individual quartz porphyroclast is a sequential process involving both subgrain/grain rotation and grain-boundary migration. Recrystallization initiates by subgrain polygonization on a single slip system (e.g. basal-*a*). This accommodates only small strains and quickly develops into subgrain rotation, with the preservation of polygonized subgrains restricted to grain interiors (cores). Continued rotation to achieve large misorientations requires more than one active slip system (e.g. basal-*m*, 'basal-prism'). Thus, for much of the recrystallization history, the grain microstructure consists of rotated subgrains and neoblasts. However, this microstructure is not necessarily stable. The relatively small subgrain and/or neoblast grain sizes result in locally high dislocation densities (e.g. boundary walls) and potentially large 'internal' strain energies. These high energies may be sufficient to initiate migration of grain boundaries and hence the preferential growth of some neoblast grains. The later stages of grain recrystallization are therefore characterized by the increasing significance of migration and the concomitant diminishing role of rotation.

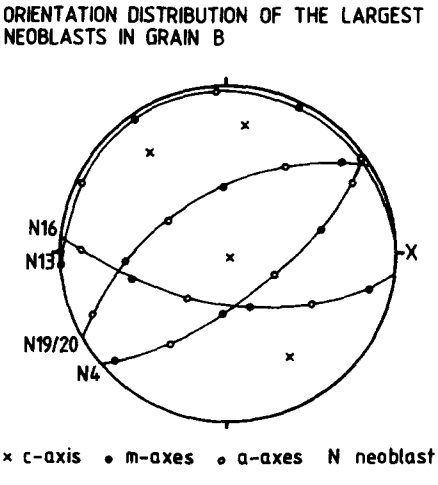

Fig. 8. Combined single crystal pole figure for the exceptionally large neoblasts (**4**, **13**, **16**, **19** and **20**). The crystal axes orientations are non-coincident and cannot be explained by a common dispersion slip system sequence. We propose that they formed by grain-boundary migrational process. Tectonic axes: *X*, E–W; *Y*, vertical; *Z*, N–S.

Acknowledgements—Financial and logistical support was provided by: U.K. Natural Environment Research Council; Departments of Geology, Universities of Nottingham and Newcastle; Centre for Materials Science, University of Birmingham; Department of Earth Sciences, University of Leeds; and Centre Geologique et Geophysique, U.S.T.L., Montpellier. We are grateful to Malcolm Hall, Colin Ferguson, Niels-Henrik Schmidt, Ian and Carol McNulty, and Dave Mainprice for their individual contributions to this work. The Journal's referees, Janos Urai and Chris Wilson, are thanked for their constructive comments.

REFERENCES

Drury, M. R., Humphreys, F. J. and White, S. H. 1985. Large strain deformation studies using polycrystalline magnesium as a rock analogue. Part II: Dynamic recrystallization mechanisms at high temperatures. *Phys. Earth & Planet. Interiors* **40**, 208–222.

Freeman, B. 1984. A method for quantitatively analysing dynamic recrystallization in deformed quartzitic rocks. *J. Struct. Geol.* **6**, 655–662.

Freeman, B. 1985. Unpublished Ph.D. thesis, University of Nottingham, U.K.

Hall, M. G. & Skinner, G. K. 1978. A spiral scanning attachment for electron channelling studies with a scanning electron microscope. *J. Phys. E* **11**. 1129–1132.

Hobbs, B. E. 1968. Recrystallization of single crystals of quartz. *Tectonophysics* **6**, 353–401.

Joy, D. C., Newbury, D. E. & Davidson, D. L. 1982. Electron channelling patterns in the scanning electron microscope. *J. appl. Phys.* **53**, R82–R122.

Lloyd, G. E. 1987. Atomic number and crystallographic contrast images with the SEM: a review of backscattered electron techniques. *Mineralog. Mag.* **51**, 3–19.

Lloyd, G. E. & Ferguson, C. C. 1986. A spherical electron channelling pattern map for use in quartz petrofabric analysis. *J. Struct. Geol.* **8**, 517–526.

Lloyd, G. E. Ferguson, C. C. & Law, R. D. 1987. Discriminatory petrofabric analysis of quartz rocks using SEM electron channelling. *Tectonophysics* **135**, 243–249.

Lloyd G. E., Schmidt, N. H., Mainprice, D. & Prior, D. J. 1991. Crystallographic textures. *Mineralog. Mag.* **55**.

Ransom, D. M. 1971. Host control of recrystallized quartz grains. *Mineralog. Mag.* **38**, 83–88.

Schmidt, N. H. & Olesen, N. O. 1989. Computer-aided determination of crystal-lattice orientation from electron-channelling patterns in the SEM. *Can. Mineralogist* **27**, 15–22.

Urai, J. L., Means, W. D. & Lister, G. S. 1986. Dynamic recrystallization of minerals. In: *Mineral and Rock Deformation: Laboratory Studies, The Paterson Volume* (edited by Hobbs B. E. & Heard H. C.) *Am. Geophys. U. Geophys. Monogr.* **36**, 161–199.

Wilson, C. J. L. 1973. The prograde microfabric in a deformed quartzite sequence, Mount Isa, Australia. *Tectonophysics* **19**, 39–81.